Physics in Medicine & Biology

IPEM Institute of Physics and Engineering in Medicine

PAPER • OPEN ACCESS

Automatic planning for functional lung avoidance radiotherapy based on function-guided beam angle selection and plan optimization

To cite this article: Tianyu Xiong *et al* 2024 *Phys. Med. Biol.* **69** 155007

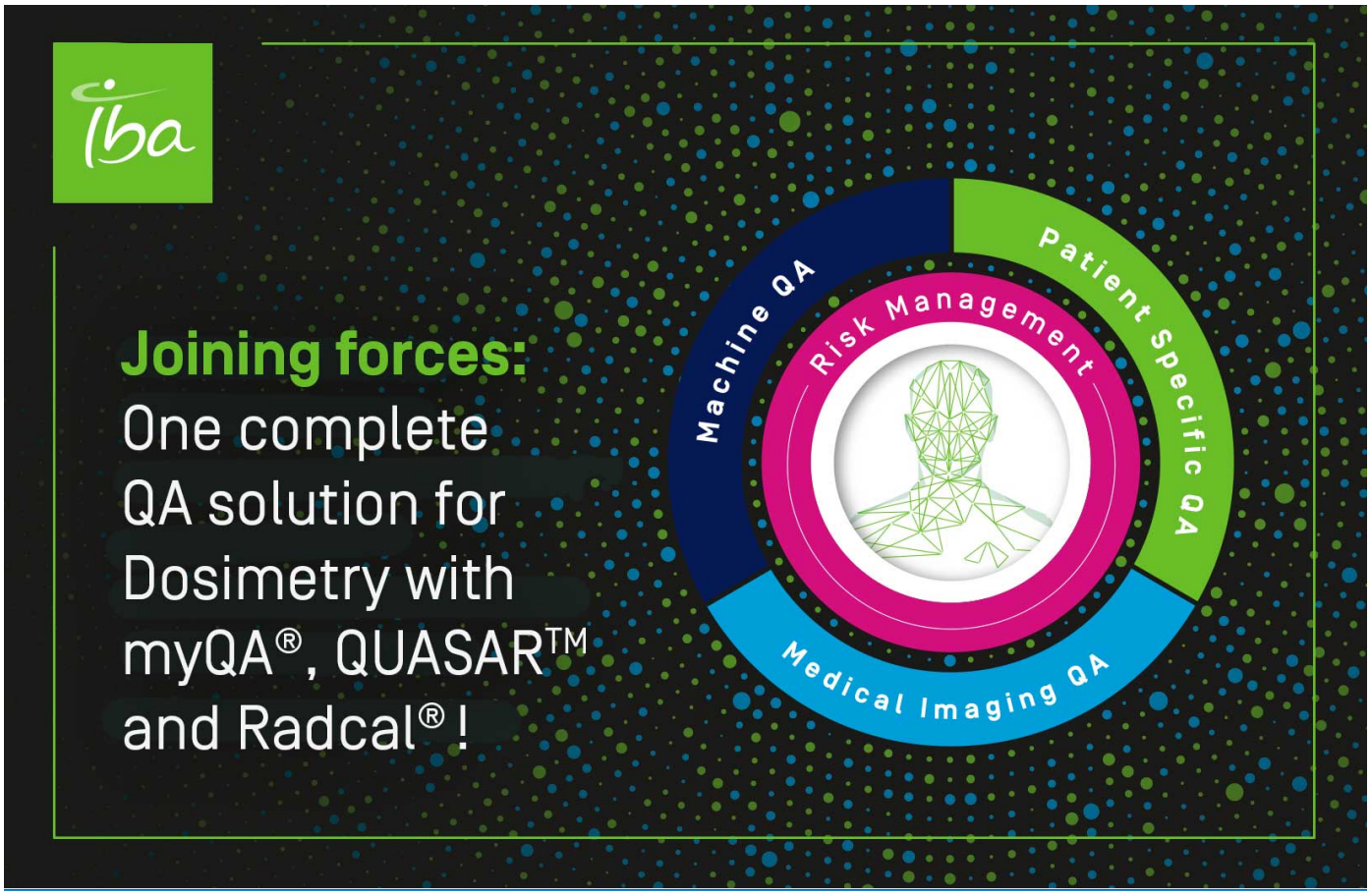

IOP Publishing Phys. Med. Biol. 69 (2024) 155007 https://doi.org/10.1088/1361-6560/ad5ef5

Physics in Medicine & Biology

IPEM Institute of Physics and Engineering in Medicine

OPEN ACCESS

RECEIVED
28 March 2024

REVISED
19 June 2024

ACCEPTED FOR PUBLICATION
3 July 2024

PUBLISHED
17 July 2024

PAPER

Automatic planning for functional lung avoidance radiotherapy based on function-guided beam angle selection and plan optimization

Tianyu Xiong[1], Guangping Zeng[1], Zhi Chen[1], Yu-Hua Huang[1], Bing Li[2], Dejun Zhou[1], Xi Liu[1], Yang Sheng[3], Ge Ren[1], Qingrong Jackie Wu[3], Hong Ge[2,*] and Jing Cai[1,*]

[1] Department of Health Technology and Informatics, The Hong Kong Polytechnic University, Hong Kong Special Administrative Region of China, People's Republic of China
[2] Department of Radiation Oncology, The Affiliated Cancer Hospital of Zhengzhou University and Henan Cancer Hospital, Zhengzhou, People's Republic of China
[3] Department of Radiation Oncology, Duke University Medical Center, Durham, NC, United States of America
[*] Authors to whom any correspondence should be addressed.

E-mail: zlyygehong0199@zzu.edu.cn and jing.cai@polyu.edu.hk

Keywords: functional lung avoidance radiotherapy, automatic planning, beam angle selection, plan optimization

Abstract

Objective. This study aims to develop a fully automatic planning framework for functional lung avoidance radiotherapy (AP-FLART). *Approach.* The AP-FLART integrates a dosimetric score-based beam angle selection method and a meta-optimization-based plan optimization method, both of which incorporate lung function information to guide dose redirection from high functional lung (HFL) to low functional lung (LFL). It is applicable to both contour-based FLART (cFLART) and voxel-based FLART (vFLART) optimization options. A cohort of 18 lung cancer patient cases underwent planning-CT and SPECT perfusion scans were collected. AP-FLART was applied to generate conventional RT (ConvRT), cFLART, and vFLART plans for all cases. We compared automatic against manual ConvRT plans as well as automatic ConvRT against FLART plans, to evaluate the effectiveness of AP-FLART. Ablation studies were performed to evaluate the contribution of function-guided beam angle selection and plan optimization to dose redirection. *Main results.* Automatic ConvRT plans generated by AP-FLART exhibited similar quality compared to manual counterparts. Furthermore, compared to automatic ConvRT plans, HFL mean dose, V_{20}, and V_5 were significantly reduced by 1.13 Gy ($p < .001$), 2.01% ($p < .001$), and 6.66% ($p < .001$) respectively for cFLART plans. Besides, vFLART plans showed a decrease in lung functionally weighted mean dose by 0.64 Gy ($p < .01$), fV_{20} by 0.90% ($p = 0.099$), and fV_5 by 5.07% ($p < .01$) respectively. Though inferior conformity was observed, all dose constraints were well satisfied. The ablation study results indicated that both function-guided beam angle selection and plan optimization significantly contributed to dose redirection. *Significance.* AP-FLART can effectively redirect doses from HFL to LFL without severely degrading conventional dose metrics, producing high-quality FLART plans. It has the potential to advance the research and clinical application of FLART by providing labor-free, consistent, and high-quality plans.

1. Introduction

Lung cancer, with an estimated 2.2 million new cases and 1.8 million deaths per year, remains the leading cause of cancer-related morbidity and mortality globally (Sung *et al* 2021, Thai *et al* 2021). Radiotherapy (RT) serves as a crucial treatment modality for lung cancer (Vinod and Hau 2020). However, radiation-induced lung injury (RILI), such as radiation pneumonitis, is a common complication of lung RT and can affect the prognosis and life quality of patients (Hanania *et al* 2019). Functional lung avoidance radiotherapy (FLART) shows promise in reducing RILI by leveraging the heterogeneity of lung function

distribution to selectively minimize dose to high functional lung (HFL) regions, thereby potentially enhancing lung function protection (Christian *et al* 2005, McGuire *et al* 2006, Ireland *et al* 2016, Faught *et al* 2017, Bucknell *et al* 2018, Vinogradskiy *et al* 2022, Zhou and Zhang 2022, Li *et al* 2023, Yamamoto *et al* 2023), in contrast to conventional anatomical image-guided RT which uniformly treats lung without function guidance.

The key to RT is to deliver high and homogeneous enough doses to planning target volume (PTV) while minimizing doses to organs at risk (OARs). FLART additionally aims to redirect dose from HFL regions to low functional lung (LFL) regions while maintaining other conventional planning criteria (Matuszak *et al* 2016). There are two effective venues to achieve dose redirection. The first one is to select beam angles that preferentially spare HFL regions prior to plan optimization, which has been proven effective in reducing doses to HFL (Tahir *et al* 2017). Another commonly used method is to modulate fluence maps by incorporating functional dose objectives in plan optimization to decrease doses to HFL (Christian *et al* 2005). The strategies of incorporating functional dose objectives can be divided into two categories: the contour-based strategy in which a HFL volume is contoured and dose-volume histogram (DVH) metrics of HFL are considered (Christian *et al* 2005); and the voxel-based strategy in which a functional weight is assigned to each lung voxel and dose-function histogram (DFH) metrics of the functionally weighted lung (FWL) are used. The choice between the two strategies remains debated, due to the lack of an established HFL definition for the contour-based strategy and the limitations of current commercial treatment planning systems (TPSs) in implementing the voxel-based strategy.

Currently, most FLART studies have employed manual planning (McGuire *et al* 2006, Ireland *et al* 2016, Yamamoto *et al* 2016, 2023, Bucknell *et al* 2018, Vinogradskiy *et al* 2022, Li *et al* 2023), which requires manually setting beam angles and iteratively adjusting plan hyperparameters in plan optimization to achieve the FLART planning goal. This labor-intensive process is dependent on the planner's experience while it is relatively scarce for the emerging FLART technique (Faught *et al* 2018). Besides, unlike anatomical OARs that exhibit great similarity in population, the lung function distributions are highly variable and patient-specific, making it more challenging for planners to select appropriate beam angles and estimate achievable dose objectives. Consequently, manual planning may require considerable time and effort and yet could still produce inconsistent or suboptimal FLART plans (Ge and Wu 2019, Moore 2019). Thus, it is necessary to develop an automatic planning (auto-planning) method for FLART to streamline the beam angle selection and plan optimization process, enhancing FLART planning efficiency, consistency, and quality.

There are very few existing studies in the realm of auto-planning for FLART. To select high-quality beam angles for FLART, McGuire *et al* (2010) proposed a beam angle selection method based on orientation and DFH contributions. Bedford and Ahmed (2023) evaluated the quality of each beam angle through conformal beam-based dose calculations and mean FWL doses. As for automatic plan optimization, Matuszak *et al* (2016) implemented a priority-driven optimization algorithm to sequentially optimize various functional and conventional dose objectives strictly following a predefined priority list. Faught *et al* (2018) trained a knowledge-based planning (KBP) model to predict optimal plan hyperparameters for FLART.

Though effective dose reduction in HFL has been achieved by these existing methods, they suffer from a few limitations. First, the performance of the KBP model is contingent upon the number and quality of training data, a significant hurdle given FLART's emerging status and the scarcity of high-quality FLART plans. The other approaches solely or excessively focus on minimizing doses to HFL, which may severely underachieve conventional dose objectives (Matuszak *et al* 2016). Currently, the clinical benefits of HFL dose reduction still desire further clinical validation (Bucknell *et al* 2018, Yaremko *et al* 2022). Therefore, minimizing functional dose metrics with excessive compromises in conventional dose metrics is undesirable (Matuszak *et al* 2016, Bucknell *et al* 2018). Besides, these studies focus on either beam angle selection or plan optimization for FLART, without offering a fully auto-planning framework. In addition, none of these studies achieve auto-planning for both the contour-based FLART (cFLART) and the voxel-based FLART (vFLART).

In this study, we aim to propose a fully auto-planning framework for FLART (AP-FLART) to address the aforementioned challenges. AP-FLART integrates and extends a dosimetric score-based beam angle selection method and a meta-optimization-based plan hyperparameter optimization approach, which can incorporate lung function information and balance conventional and functional dose objectives to facilitate dose redirection in the beam angle selection phase and the plan optimization phase respectively (Yuan *et al* 2018, Huang *et al* 2022a). Different from the existing methods, AP-FLART is training data-free and can comprehensively consider functional and conventional dose metrics to achieve dose redirection from HFL to LFL while minimizing compromises in conventional metrics. Besides, it can automate the whole planning process and generate plans for both cFLART and vFLART. In addition to FLART plans, AP-FLART can also produce conventional RT (referred to ConvRT) plans so that clinicians can explicitly evaluate the gain of better lung function protection and the potential cost of inferior conventional metrics following the current

routine of FLART studies (Vinogradskiy *et al* 2022). The proposed AP-FLART shall advance the research and clinical application of FLART by providing labor-free, consistent, and high-quality FLART plans.

2. Method

Figure 1 depicts an overview of this study. AP-FLART can generate ConvRT, cFLART, and vFLART plans by sequentially determining beam angle configurations, optimizing dose objective weights, and generating final plans. The beam angle selection method employs beam quality evaluation guided by beamlet-wise dose calculations and a beam score function. The plan hyperparameter optimization method optimizes the weights of different dose objectives by navigating the Pareto front guided by a plan score function. Notably, unlike ConvRT planning which solely utilizes anatomical information and considers anatomical dose objectives, FLART planning additionally utilizes lung function information and incorporates functional dose objectives into the beam angle selection and plan optimization processes. Consequently, beam angles that originally irradiate HFL in ConvRT plans tend to be deflected to irradiate LFL, and intensities of beamlets irradiating HFL in ConvRT plans tend to be diverted to those irradiating LFL, both contributing to dose redirection from HFL to LFL. A cohort of patient data was collected for the development and validation of AP-FLART. For all collected patient cases, AP-FLART was applied to generate ConvRT, cFLART, and vFLART plans and the results were compared to evaluate the performance of AP-FLART.

2.1. Patient data and preprocessing

A total of 18 lung cancer patient cases underwent SPECT/CT scans and intensity modulated radiation therapy (IMRT) were retrospectively collected from the Affiliated Cancer Hospital of Zhengzhou University with approval by the institutional review board. All cases contain perfusion SPECT/CT images, planning CT images, PTV and OARs contours, and conventional IMRT plans. All conventional IMRT plans were made using the Eclipse (Varian Medical Systems, Palo Alto, CA, USA) TPS with the analytical anisotropic algorithm dose engine and dynamic IMRT technique. The radiopharmaceutical technetium-99m-labeled macroaggregated albumin (MAA) was injected into patients and then 3D perfusion SPECT/CT scans were acquired using a GE Discovery NM/CT 670 CZT scanner (GE HealthCare, Chicago, IL, USA). A total of 60 frames were acquired for each patient with a frame rate of 10 s per frame. The SPECT images had dimensions of $128 \times 128 \times 128$ with a voxel size of $4.42 \times 4.42 \times 4.42$ mm^3, respectively. The planning CT images had an in-slice resolution of 1.172 mm and a slice thickness of 3 mm. The planning CT and SPECT/CT images were acquired under free-breathing conditions.

The principle of SPECT perfusion imaging is that the labeled MAA particles will be lodged within the pulmonary capillary beds and their local concentration is directly related to the regional pulmonary blood flow (McGuire *et al* 2006). The SPECT scanner can detect the distribution of these trapped MAA particles and generate SPECT perfusion images, which can quantify lung perfusion function distribution and serve as a surrogate for lung function (Bria *et al* 1983, McGuire *et al* 2006, Hoover *et al* 2014, Khalil *et al* 2021). Therefore, this study utilized SPECT perfusion images to guide FLART planning. As shown in figure 2, the attenuation corrected CT images from SPECT/CT were first registered with the planning CT images using rigid registration, and the resulting transformations were applied to register the SPECT images with the planning CT images (Matuszak *et al* 2016). All registration operations were performed within MIM platform (MIM Software Inc., Cleveland, OH, USA). Threshold segmentation with a cutoff value of 66th percentile (Yamamoto *et al* 2011, Ren *et al* 2021) was then performed on the registered SPECT images to generate HFL contours. The intensity values of SPECT images were normalized to the mean intensity value within the lung contour to obtain FWL maps (Matuszak *et al* 2016).

2.2. Function-guided dosimetric score-based beam angle selection

A novel function-guided beam angle selection method is developed by extending the dosimetric score-based method originally proposed for conventional lung IMRT by Yuan *et al* (2018) The original method evaluates beam angle qualities by using beamlet-wise dose calculations and anatomical information. Our enhancement differs from the original one by comprehensively utilizing both anatomical and functional information, aiming to deflect beam angles from HFL to LFL.

The quantitative evaluation of each beam is based on beamlet-wise comparison. For each beam angle, this process involves computing dose distributions of each beamlet and then quantifying the beamlet's quality by calculating a function-aware beamlet-wise quality score. The beam score (bs) functions for ConvRT, cFLART and vFLART are defined as follows:

$$bs_{\alpha i} = \frac{\sum_{jOAR} w^{jOAR} \sum_{k \in jOAR} d^k_{\alpha i} + w^{NT} \sum_{k \in NT} d^k_{\alpha i}}{\sum_{k \in PTV} d^k_{\alpha i}}, \text{ for } ConvRT \quad (1)$$

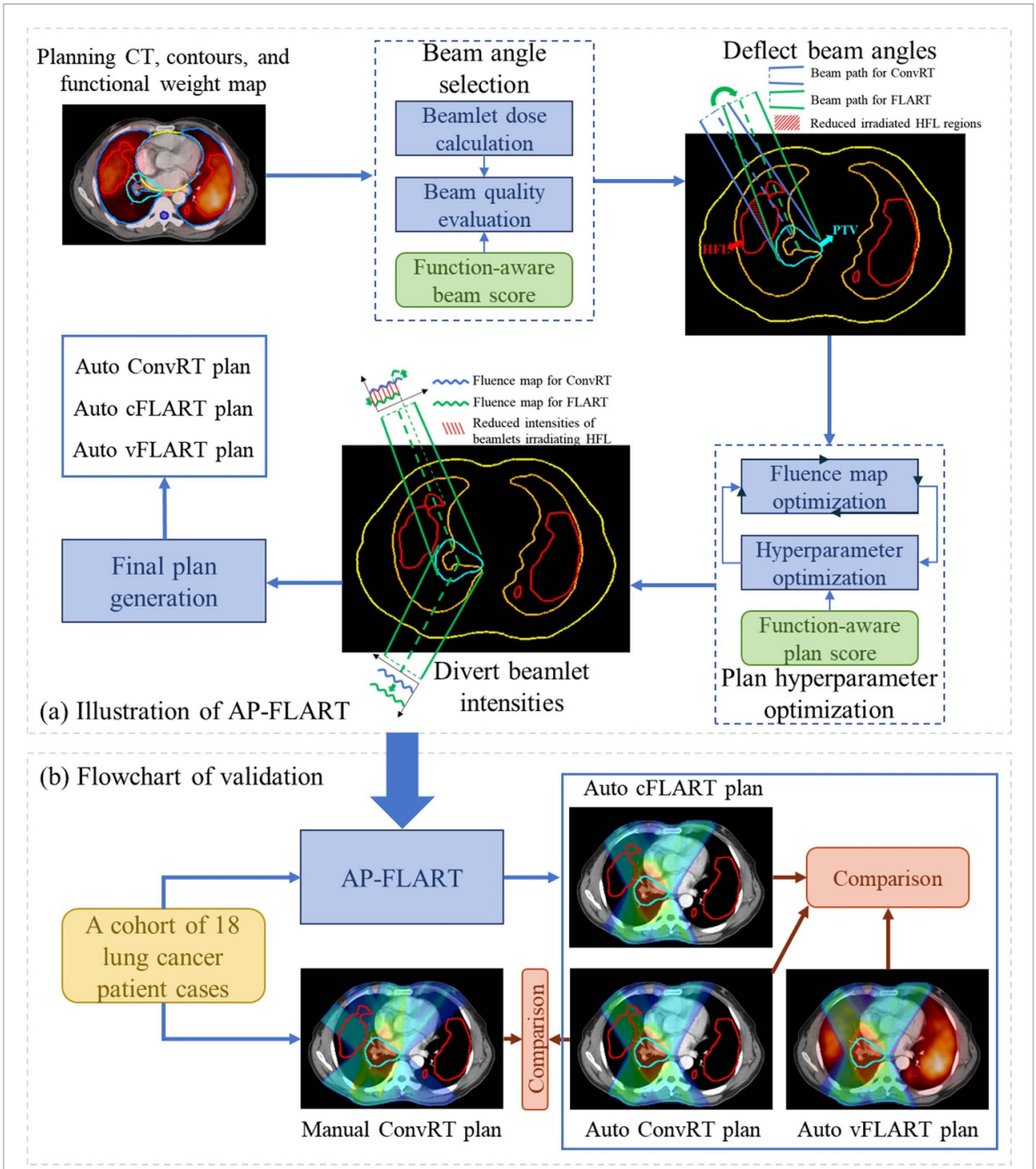

Figure 1. The overview of this study including (a) the illustration of the proposed AP-FLART and (b) the flowchart of its validation.

$$bs_{\alpha i} = \frac{\sum_{jOAR} w^{jOAR} \sum_{k \in jOAR} d^k_{\alpha i} + w^{NT} \sum_{k \in NT} d^k_{\alpha i} + w^{HFL} \sum_{k \in HFL} d^k_{\alpha i}}{\sum_{k \in PTV} d^k_{\alpha i}}, \text{for } cFLART \tag{2}$$

$$bs_{\alpha i} = \frac{\sum_{jOAR} w^{jOAR} \sum_{k \in jOAR} d^k_{\alpha i} + w^{NT} \sum_{k \in NT} d^k_{\alpha i} + w^{FWL} \sum_{k \in FWL} f^k d^k_{\alpha i}}{\sum_{k \in PTV} d^k_{\alpha i}}, \text{for } vFLART \tag{3}$$

where $bs_{\alpha i}$ is the function-aware quality score for the beamlet i of the beam α. $d^k_{\alpha i}$ represents doses irradiated by the beamlet to voxel k of OARs, normal tissues (NTs), HFL, FWL and PTV. The weights including w^{jOAR}, w^{NT}, w^{HFL}, and w^{FWL} reflect the relative importance of different regions to be protected. f^k refers to the functional weight value of voxel k in FWL. A lower $bs_{\alpha i}$ indicates a preferred balance of minimizing doses to protected areas while delivering high enough doses to PTV, marking a beamlet as of high quality. Different from $bs_{\alpha i}$ for ConvRT, $bs_{\alpha i}$ for cFLART additionally includes a HFL term and $bs_{\alpha i}$ for vFLART replaces the lung term with a FWL term. The details are provided in appendix A. The quality of each individual beam is then quantified by calculating a beam-wise quality score (bs_α), the average of all beamlet-wise quality scores.

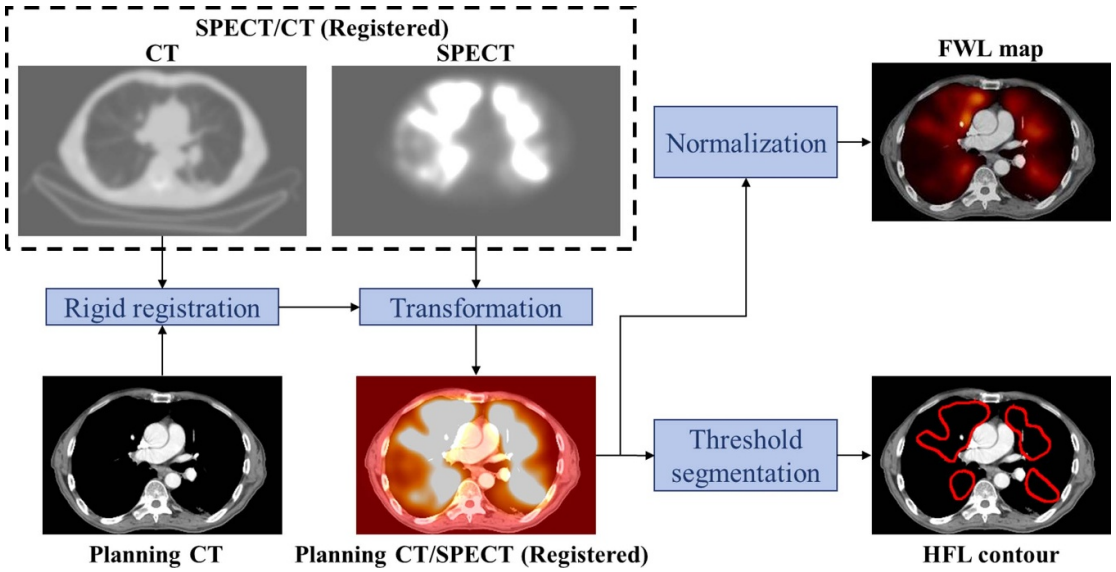

Figure 2. The flowchart of data preprocessing including the registration between SPECT and planning CT as well as the generation of FWL maps and HFL contours.

In addition to the quality of individual beams, the collective effects of multiple beams should also be considered. Clinical insights suggest that overly condensed beam angle distributions may lead to poor plan quality (Meyer *et al* 2005, Amit *et al* 2015, Yuan *et al* 2018). Therefore, a beam span constraint is introduced when selecting beam angles (Yuan *et al* 2015, 2018). The optimized beam angle configuration is selected by minimizing the following objective function:

$$OF_{\Pi} = \sum_{\alpha_i \in \Pi} bs_{\alpha_i} + \sum_{\alpha_i, \alpha_j \in \Pi; \alpha_i \neq \alpha_j} \frac{2k}{1-\cos\left(\left|\alpha_i - \alpha_j\right|\right)+\delta} \tag{4}$$

where α_i and α_j represent two different beam angles in the beam angle configuration Π. The objective function consists of two terms: a sum of all beam-wise quality scores reflecting the individual quality of selected beam angles and a beam span term discouraging tightly clustered beam configurations. k stands for the weight of the beam span term and δ is a regularization parameter. The beam angle search space will be constrained to coplanar orientations, with candidate angles sampled at 5-degree intervals. The selected beam angle configuration, denoted as Π, will be initialized as an empty set. For each iteration of the optimization process, the beam angle search space will be traversed to identify the specific angle that results in the smallest incremental increase in the objective function, OF_{Π}. This optimal beam angle will then be added to the selected configuration Π, and both this angle and its opposing angle will be removed from the remaining search space following clinical practice. This iterative process will continue until the total number of selected beam angles reaches the predefined target number, which is set to be 8 following the (Yuan *et al* 2018).

The angle selection method involves several parameters to be determined, including the weights of different regions to be protected as well as the weight and regularization parameter of the beam span term of equation (4). For ConvRT, these parameters were fine-tuned based on the results from Yuan *et al* (2018). The weights for the anatomical/functional lung term for FLART were then further fine-tuned to minimize functional dose metrics while maintaining conventional dose metrics. The details of parameter determination are presented in appendix A.

2.3. Function-guided meta-optimization-based plan optimization

The meta-optimization framework, proven to be effective for conventional head and neck as well as prostate RT planning (Huang *et al* 2022a), is further enhanced in this study for FLART plan hyperparameter optimization. As a multi-criteria optimization-based approach, the original meta-optimization method navigates the Pareto front to identify plans that achieve a balance between different conventional dose objectives guided by a plan score involving important conventional metrics. In this study, we accommodate the approach to lung RT and extend it by incorporating additional lung function information to facilitate dose redirection for FLART. We also accelerate the framework by designing a novel initialization method to ensure the computation time is clinically acceptable.

The meta-optimization framework consists of two nested loops of optimization as demonstrated in figure 3. In the inner loop, fluence map optimization (FMO) is performed to generate Pareto optimal plans

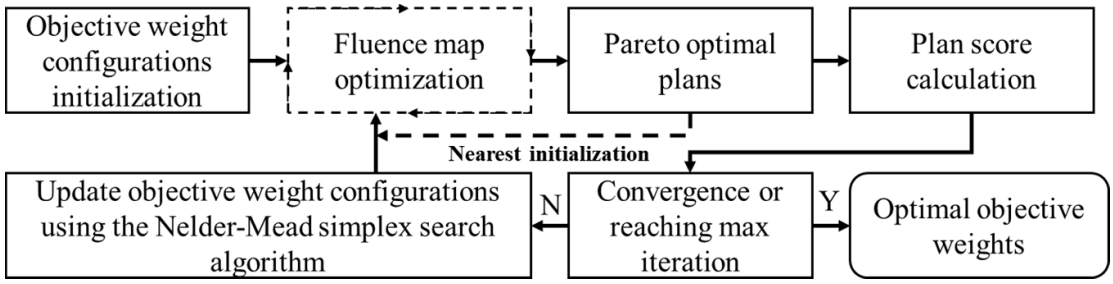

Figure 3. Flowchart of meta-optimization-based plan hyperparameter optimization.

by minimizing the weighted sum of conventional dose objectives and potential functional dose objectives as formulated by the following equations:

$$\min_{x} \quad \frac{w_{PTV}}{N_{PTV}} \sum_{i \in PTV} (d_i - D_p)^2 + \sum_{S \in OARs} \frac{w_S}{N_s} \sum_{i \in S} H(d_i - D_s)\,(d_i - D_s)^2, \text{ for } ConvRT \tag{5}$$

$$\frac{w_{PTV}}{N_{PTV}} \sum_{i \in PTV} (d_i - D_p)^2 + \sum_{S \in OARs} \frac{w_S}{N_s} \sum_{i \in S} H(d_i - D_s)\,(d_i - D_s)^2 + \frac{w_{HFL}}{N_{HFL}} \sum_{i \in HFL} H(d_i - D_{HFL})\,(d_i - D_{HFL})^2, \text{ for } cFLART \tag{6}$$

$$\frac{w_{PTV}}{N_{PTV}} \sum_{i \in PTV} (d_i - D_p)^2 + \sum_{S \in OARs} \frac{w_S}{N_s} \sum_{i \in S} H(d_i - D_s)\,(d_i - D_s)^2 + \frac{w_{FWL}}{N_{FWL}} \sum_{i \in FWL} H(d_i - D_{FWL})\, f_i (d_i - D_{FWL})^2, \text{ for } vFLART$$

$$\text{s.t.} \quad x \geqslant 0, \quad w \geqslant 0, \quad \vec{d} = D\vec{x} \tag{7}$$

where $\vec{x}$, D, and $\vec{d}$ refer to the fluence map, the dose influence matrix, and the dose distribution respectively. d_i and f_i represent the dose value and the functional weight value of voxel i respectively. w and N are the weights of different objectives and the number of voxels in different regions respectively. D_p, D_s, D_{HFL}, and D_{FWL} stand for reference dose of different objectives. H represents the Heaviside function. The details of dose objectives are summarized in table 1.

In the outer loop, the gradient-free Nelder–Mead simplex search algorithm (Nelder and Mead 1965, Lee and Wiswall 2007, Huang *et al* 2022a) is applied to iteratively optimize the weights of different objectives (w) to minimize a function-aware plan quality score (ps). This plan score (ps) integrating several plan quality metrics of clinical importance is used to quantify the clinical acceptability of different Pareto optimal plans generated from the inner loop. The outer loop is formulated as:

$$\begin{aligned} &\min_{w} \quad ps(w) = \sum_{QM} 2^{-P_{QM}} F_{QM} \\ &\text{s.t.} \quad\quad w \geqslant 0 \\ &F_{QM} = \begin{cases} 1, & QM \geqslant QM_+ \\ \frac{QM - QM_-}{QM_+ - QM_-}, & QM_- < QM < QM_+ \\ 0, & QM \leqslant QM_- \end{cases} \end{aligned} \tag{8}$$

where the P_{QM} and F_{QM} refer to the priorities and scoring values of different quality metrics (QM). The relationship between the score values and the QM values is formulated as a clipped linear function, and the linear range is defined as $[QM_-\ QM_+]$. The quality metrics of different structures and their priorities as well as linear ranges are enumerated in table 1. Among them, functional dose metrics including mean dose, V_5, and V_{20} for HFL, as well as functionally weighted mean dose, fV_5, fV_{20} for FWL are utilized for FLART because they are widely used in FLART studies (Yamamoto *et al* 2016, Faught *et al* 2017, Vinogradskiy *et al* 2022). The other conventional dose metrics are extracted from the Radiation Therapy Oncology Group 0617 protocol and are commonly used in clinical plan evaluation (Bradley *et al* 2015, Yamamoto *et al* 2016, Yuan *et al* 2018, Yaremko *et al* 2022, Li *et al* 2023). Additionally, a novel nearest initialization method was introduced to accelerate the meta-optimization framework, achieving a 63% reduction in computation time, with details presented in appendix B. The implementation details of the meta-optimization framework including weight configuration initialization, convergence conditions, and so on are presented in the (Huang *et al* 2022a).

Table 1. The details of the dose objectives used in the inner loop, the quality metrics involved in the outer loop, and the dose constraints for OARs considered in evaluation.

Structure	Reference dose (Gy)	Quality metric (QM)	$QM-$	$QM+$	Priority	Dose constraints
			For ConvRT:			
PTV	60	HI CI	5 0.6	10 0.7	0 1	
Spinal cord	35	D_{max}	40.5 Gy	45 Gy	2	$D_{max} < 45$ Gy
Esophagus	0	D_{mean}	30.6 Gy	34 Gy	2	$D_{mean} < 34$ Gy
Heart	0	D_{mean}	40.5 Gy	45 Gy	2	$V_{40} < 30\%$ $D_{mean} < 28$ Gy
Lung	0	D_{mean} V_5 V_{20}	0 Gy 25% 0%	15 Gy 50% 25%	1 1 1	$D_{mean} < 20$ Gy $V_5 < 60\%$ $V_{20} < 30\%$
Body	30	D_{mean}	8.1 Gy	9 Gy	3	
			Changes when converting from ConvRT to cFLART:			
Lung	0	D_{mean}	18 Gy	20 Gy	2	$D_{mean} < 20$ Gy $V_5 < 60\%$ $V_{20} < 30\%$
HFL	0	D_{mean} V_5 V_{20}	0 Gy 25% 0%	15 Gy 50% 25%	1 1 1	
			Changes when converting from ConvRT to vFLART:			
Lung	None					$D_{mean} < 20$ Gy $V_5 < 60\%$ $V_{20} < 30\%$
FWL	0	fD_{mean} fV_5 fV_{20}	0 Gy 25% 0%	15 Gy 50% 25%	1 1 1	

Note: CI (conformity index) $= \frac{(TV_{95D_p})^2}{TV \times V_{95D_p}}$; HI (homogeneity index) $= \frac{D_5 - D_{95}}{D_p} \times 100$; D_p: prescription dose; D_{mean}: mean dose; D_{max}: maximal dose; V_x: portion of structure volume irradiated by dose higher than x Gy; D_x: minimum dose to the 'hottest' x% of structure volume.

Upon determining the optimal beam angles and dose objective weights, final plans are generated by sequentially performing FMO, leaf sequencing, and direct aperture optimization using the open-source TPS matRad (Wieser *et al* 2017). The pencil beam dose calculation engine of matRad (Bortfeld *et al* 1993) and static IMRT technique (Siochi 1999) are utilized in the beam angle selection and plan optimization processes. We extend matRad to enable it to incorporate the voxel-wise FWL maps and optimize the dose-function objectives of vFLART.

2.4. Evaluation and ablation studies

To evaluate the performance of AP-FLART, comparison studies were conducted by using the collected cohort. For each patient case, a ConvRT plan, a cFLART plan, and a vFLART plan were automatically devised by using AP-FLART. Dose distributions of automatic plans and collected manual plans were normalized to guarantee that the prescription dose (60 Gy) could cover 95% of PTV for consistent comparison. The analysis included comparing automated ConvRT plans with manual plans to validate the auto-planning framework's effectiveness. Since manual plans were made using Eclipse while automatic plans were generated based on matRad, to reduce discrepancies caused by using different TPSs, a voxel-based dose mimicking algorithm (McIntosh *et al* 2017, Fan *et al* 2019) was applied to convert all manual Eclipse plans to matRad plans which would be used for comparison with automatic plans. The details of applying the dose mimicking algorithm for plan conversion are presented in appendix C. Additionally, comparisons between automated FLART and ConvRT plans were executed to ascertain AP-FLART's ability of facilitating dose redirection.

There are two driving forces to achieve dose redirection in AP-FLART. The function-guided beam angle selection method can deflect beam angles irradiating HFL and the function-guided plan optimization approach can divert intensities of beamlets irradiating HFL. We conducted several ablation studies to quantify the contribution of the two driving forces. In the study 'ConvBeam_cFLART' and 'ConvBeam_vFLART', beam angles selected for ConvRT and plan hyperparameters optimized for FLART were used to generate cFLART and vFLART plans respectively. Another two studies adopted beam angles selected for cFLART and vFLART and plan hyperparameters optimized for ConvRT, and they were referred to as 'cFLARTBeam_ConvRT' and 'vFLARTBeam_ConvRT' respectively. All quality metrics listed in the table 1 were included in the evaluation criteria. In addition, D_1 of PTV, Esophagus, and Heart were also evaluated to monitor the change of hot spots.

3. Results

3.1. Comparison between manual and automatic ConvRT plans

Table 2 reveals that automatic ConvRT plans generally match the quality of manual plans. Specifically, compared to manual ConvRT plans, automatic ConvRT plans significantly enhanced five out of thirteen conventional metrics including HI, CI, PTV D_1, mean doses to lung and body while significantly increased lung V_5. The other metrics showed no statistically significant change.

3.2. Comparison between automatic ConvRT and FLART plans

Table 2 also presents comparison between automatic ConvRT and FLART plans. Compared with ConvRT plans, FLART plans significantly reduced functional dose metrics with modest compromise in conventional dose metrics. The cFLART plans showed a significant decrease by 1.13 Gy for HFL mean dose ($p < .001$), 2.01% for HFL V_{20} ($p < .001$), and 6.66% for HFL V_5 ($p < .001$), with a decrease by 5.26% for CI ($p < .01$). As for vFLART plans, FWL functionally weighted mean dose, fV_{20}, and fV_5 were reduced by 0.64 Gy ($p < .01$), 0.90% ($p = 0.099$), and 5.07% ($p < .01$) respectively while CI decreased by 6.58% ($p < .01$). Though inferior conformity was observed in FLART plans, all dose constraints listed in table 1 were well satisfied. Figure 4 compares DVH and DFH curves of automatic FLART and ConvRT plans. Lower doses to HFL and FWL were observed in cFLART and vFLART plans. The cFLART and vFLART plans demonstrated similar mean DVH for HFL and mean DFH for FWL.

Figure 5 showcases iso-dose curves of ConvRT and FLART plans in an example case. We observed effective dose redirection in cFLART and vFLART plans including dose reduction in high function regions indicated by red arrows and dose increase in low function regions indicated by blue arrows.

3.3. Ablation study results

The ablation study results are depicted in figure 6 and elaborated in table A3 of appendix D. Compared with the automatic ConvRT plans, the plans of 'cFLARTBeam_ConvRT' and 'vFLARTBeam_ConvRT' reduced HFL mean dose by 5.13% ($p = 0.099$) and FWL functionally weighted mean dose by 3.73% ($p = 0.099$) respectively. Besides, the 'ConvRTBeam_cFLART' and 'ConvRTBeam_vFLART' plans achieved a reduction in HFL mean dose by 10.82% ($p < .001$) and FWL functionally weighted mean dose by 3.49% ($p = 0.108$) respectively. With the combination of the two driving forces for shifting dose, cFLART further reduced HFL mean dose by 11.11% ($p < .001$) and 5.44% ($p < .01$) compared to the 'cFLARTBeam_ConvRT' and 'ConvRTBeam_cFLART' respectively. FWL functionally weighted mean dose further decreased by 4.12% ($p < .01$) and 4.36% ($p < .001$) in vFLART compared to the 'vFLARTBeam_ConvRT' and 'ConvRTBeam_vFLART'.

3.4. Computation time

AP-FLART was evaluated on a workstation equipped with Intel(R) Xeon(R) Gold 6226R CPUs (2.9 GHz). The voxel size of dose grid and bixel width of beamlet grid were set to be $3 \times 3 \times 3$ mm^3 and 5 mm respectively for beam angle selection. The plan hyperparameter optimization adopted dose grid and beamlet grid with a coarser resolution of $5 \times 5 \times 5$ mm^3 and 7 mm respectively for improving computation efficiency. In the final plan generation process, the voxel size of dose grid and pixel width of beamlet grid were set to be $2 \times 2 \times 2$ mm^3 and 5 mm respectively. The parallel computation with the parallel number of 8 was adopted for beam angle selection and plan hyperparameter optimization. As a result, the computation time for beam angle selection, plan hyperparameter optimization, and final plan generation was 7.7 ± 2.4 min, 36.7 ± 11.5 min, and 44.6 ± 15.4 min per plan respectively, culminating in a total computation time of 89.0 ± 26.4 min per plan.

Table 2. Comparison between manual and automatic ConvRT plans as well as comparison between automatic ConvRT and FLART plans. The mean and standard deviation of the dose metrics over all collected cases are listed. The *p*-values by Wilcoxon signed-rank test are also shown.

Dose metrics	Manual ConvRT VS Auto ConvRT			Auto FLART VS Auto ConvRT			
	Manual ConvRT	Auto ConvRT	*p*-value	Auto cFLART	*p*-value	Auto vFLART	*p*-value
HI	6.71 ± 1.76	5.56 ± 0.51	**0.030**	5.61 ± 0.52	0.304	5.55 ± 0.54	0.966
CI	0.63 ± 0.09	0.76 ± 0.06	**<0.001**	0.72 ± 0.06	**0.006**	0.71 ± 0.08	**0.004**
PTV D_1 (Gy)	64.61 ± 1.17	63.93 ± 0.35	**0.027**	64.01 ± 0.41	0.276	63.96 ± 0.43	1.000
HFL D_{mean} (Gy)	7.17 ± 2.48	7.21 ± 2.28	0.766	6.08 ± 2.44	**<0.001**	6.18 ± 2.39	0.001
HFL V_{20} (%)	12.88 ± 5.66	13.01 ± 5.55	1.000	11.00 ± 5.75	**<0.001**	11.14 ± 5.60	0.003
HFL V_5 (%)	26.63 ± 9.03	32.64 ± 10.50	0.038	25.98 ± 9.32	**<0.001**	26.30 ± 12.22	0.002
FWL fD_{mean} (Gy)	8.62 ± 2.51	8.32 ± 2.22	0.246	7.76 ± 2.44	0.010	7.68 ± 2.37	**0.009**
FWL fV_{20} (%)	15.75 ± 5.61	15.18 ± 5.23	0.284	14.71 ± 5.57	0.551	14.28 ± 5.55	0.099
FWL fV_5 (%)	30.66 ± 8.08	35.92 ± 9.27	0.014	30.69 ± 9.16	<0.001	30.85 ± 10.87	**0.005**
Lung D_{mean} (Gy)	10.59 ± 2.12	10.04 ± 2.11	**0.021**	10.05 ± 1.88	0.671	9.94 ± 2.04	0.347
Lung V_{20} (%)	19.73 ± 4.44	18.74 ± 4.59	0.130	19.56 ± 4.09	0.108	19.18 ± 4.77	0.932
Lung V_5 (%)	35.05 ± 5.76	39.79 ± 8.61	**0.007**	36.55 ± 7.74	0.007	36.26 ± 7.75	0.016
Spinal cord D_{max} (Gy)	36.63 ± 3.95	37.69 ± 6.86	0.393	38.01 ± 5.59	0.734	37.63 ± 6.47	0.468
Esophagus D_{mean} (Gy)	13.32 ± 6.39	13.29 ± 8.38	0.609	12.05 ± 7.80	0.005	12.91 ± 8.07	0.099
Esophagus D_1 (Gy)	50.93 ± 17.26	49.80 ± 21.81	0.865	48.86 ± 21.94	0.130	49.84 ± 20.23	0.054
Heart D_{mean} (Gy)	7.37 ± 5.95	6.37 ± 6.21	0.734	6.69 ± 6.38	0.799	7.03 ± 6.33	0.832
Heart D_1 (Gy)	39.27 ± 17.33	33.41 ± 23.82	0.196	33.88 ± 23.96	0.832	34.67 ± 23.71	0.196
Heart V_{40} (%)	1.92 ± 2.19	2.29 ± 2.86	0.518	2.47 ± 3.39	0.969	2.49 ± 3.02	0.784
Body D_{mean} (Gy)	4.91 ± 1.48	4.78 ± 1.55	**0.048**	4.76 ± 1.49	0.671	4.73 ± 1.50	0.130

Note: CI (conformity index) $= \frac{(TV_{95D_p})^2}{TV \times V_{95D_p}}$; HI (homogeneity index) $= \frac{D_5 - D_{95}}{D_p} \times 100$; D_p: prescription dose; D_{mean}: mean dose; D_{max}: maximal dose; V_x: portion of structure volume irradiated by dose higher than x Gy; D_x: minimum dose to the 'hottest' x% of structure volume.

4. Discussion

This study introduced an AP-FLART integrating and enhancing a dosimetric score-based beam angle selection method and a meta-optimization-based plan hyperparameter optimization method. AP-FLART can generate ConvRT plans with similar or better quality in terms of all evaluated conventional metrics except for lung V_5 compared to manual plans, validating the effectiveness of the proposed auto-planning method. The higher lung V_5 of automatic plans is a compromise to achieve better PTV homogeneity and conformity. Besides, the increased lung V_5 ($39.79 \pm 8.61\%$) is well below the dose constraints (60%). Furthermore, AP-FLART is capable of taking into account lung functional information in both beam angle selection and plan optimization phases using either the contour-based or voxel-based strategy and generating FLART plans. Compared with the automatic ConvRT plans, the automatic FLART plans significantly reduced HFL mean dose, V_5, and V_{20} by 1.13 Gy, 6.66%, and 2.01%, as well as FWL functionally weighted mean dose, fV_5, and fV_{20} by 0.64 Gy, 5.07%, and 0.90% respectively, which could potentially better protect patients' lung function and reduce the risk of pulmonary side effects (Faught *et al* 2017). The reduction in the functional dose metrics is similar to existing FLART planning studies. Yaremko *et al* achieved a reduction in HFL mean dose, V_5, and V_{20} by 1.0 Gy, 3.5%, and 2.9% respectively (2022). Vinogradskiy *et al* reported that HFL mean dose, V_5, and V_{20} were reduced by 1.4 Gy, 3.4%, and 3.5% respectively (2022). In the study by Yamamoto *et al* FWL functionally weighted mean dose and fV_{20} decreased by 0.5 Gy and 3.8% respectively (2023).

In addition to reducing functional dose metrics, FLART also aims to minimize compromises in conventional dose metrics (Matuszak *et al* 2016, Bucknell *et al* 2018). For Pareto optimal plans, dose reduction in HFL will inevitably result in dose increase in other regions. Ideally, FLART redirects these doses from HFL to LFL instead of affecting other OARs, thus preserving conventional dose metrics. According to the results presented in table 2, the automatic FLART plans significantly reduced HFL mean dose and FWL functionally weighted mean dose while maintaining anatomical lung mean dose similar, indicating an effective dose shift from HFL to LFL as demonstrated in figure 5 as well. Though a reduction in conformity was observed, none of the other conventional dose metrics changed significantly. The conformity losses, often observed in FLART studies (Yamamoto *et al* 2011, Huang *et al* 2013, Matuszak *et al* 2016), due to lung function's anisotropic distribution around PTV, are considered as a common trade-off for dose redirection.

The ablation study results demonstrate that the function-guided beam angle selection and plan optimization jointly contributed to dose redistribution. Distinct from the functional dose metrics-oriented beam angle selection methods proposed by McGuire *et al* and Bedford *et al* which solely or excessively pursue

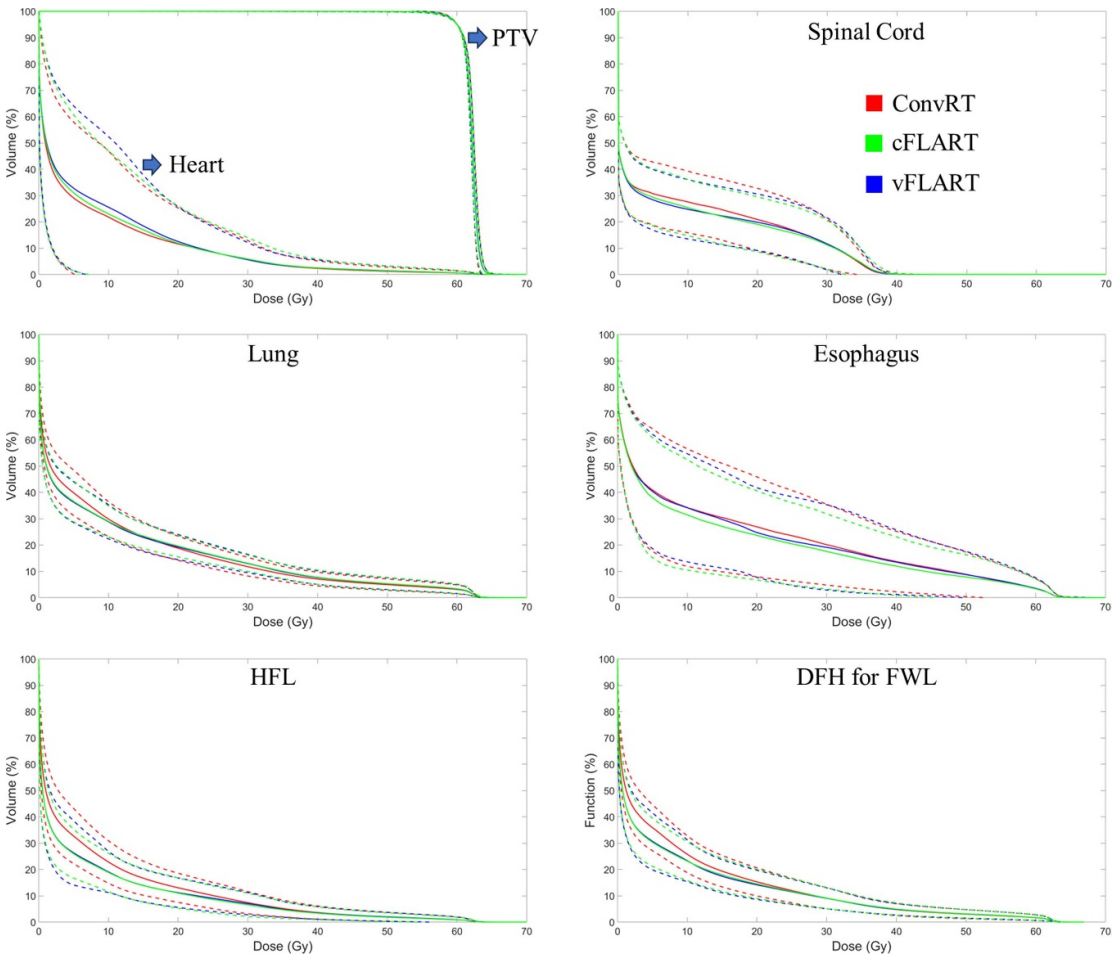

Figure 4. Comparison of DVH for different structures and DFH for FWL among automatic ConvRT plans (red), cFLART plans (green), and vFLART plans (blue). The solid lines and dashed lines represent the means and the standard deviations over all collected cases.

optimal lung function protection (2010, 2023), our proposed beam angle selection method features in comprehensively considering both functional and conventional dose metrics, therefore advancing in minimizing compromises in conventional dose metrics. This is achieved by utilizing a function-aware beam score function to guide the beam selection process. The weights of different protected regions in the score function represent their relative importance. In the transition from ConvRT to FLART, the weights of conventional OARs remain constant, and the relative weight of the anatomical/functional lung term is maintained. Consequently, beams originally irradiating HFL in ConvRT plans are preferably deflected to LFL instead of other OARs.

In the plan optimization phase, incorporating functional dose objectives can reduce doses to HFL. We adapted and enhanced the meta-optimization-based approach to optimize the weights of conventional and functional dose objectives to achieve a balance. Compared to the priority-driven approach (Matuszak *et al* 2016) which results in statistically significant dose increase in heart, spinal cord, and esophagus, our method better maintains the conventional dose metrics. A small compromise in functional dose metrics may potentially considerably improve conventional dose metrics, and such a compromise will be preferably made in clinical practice. However, the priority-driven approach fails to do so as it strictly follows a priority list and the priority of minimizing doses to functional lung is higher than conventional OARs. In contrast, the meta-optimization-based approach is more flexible and small compromises in functional dose metrics can be made only if they are clinically beneficial indicated by a lower plan score.

Given the absence of established protocols for FLART currently, much effort is being made to develop a standardized protocol (Ireland *et al* 2016, Bucknell *et al* 2018). AP-FLART can assist FLART research by providing labor-free, high-quality, and consistent FLART plans. For example, there are some controversies about which kind of patients may benefit from FLART. The study by Li *et al* (2023) reported that patients with PTV surrounded by HFL may gain more dosimetric benefits from FLART plans while Munawar *et al* observed inconsistent results (2010). The work by Christian *et al* (2005) concluded that patients with one

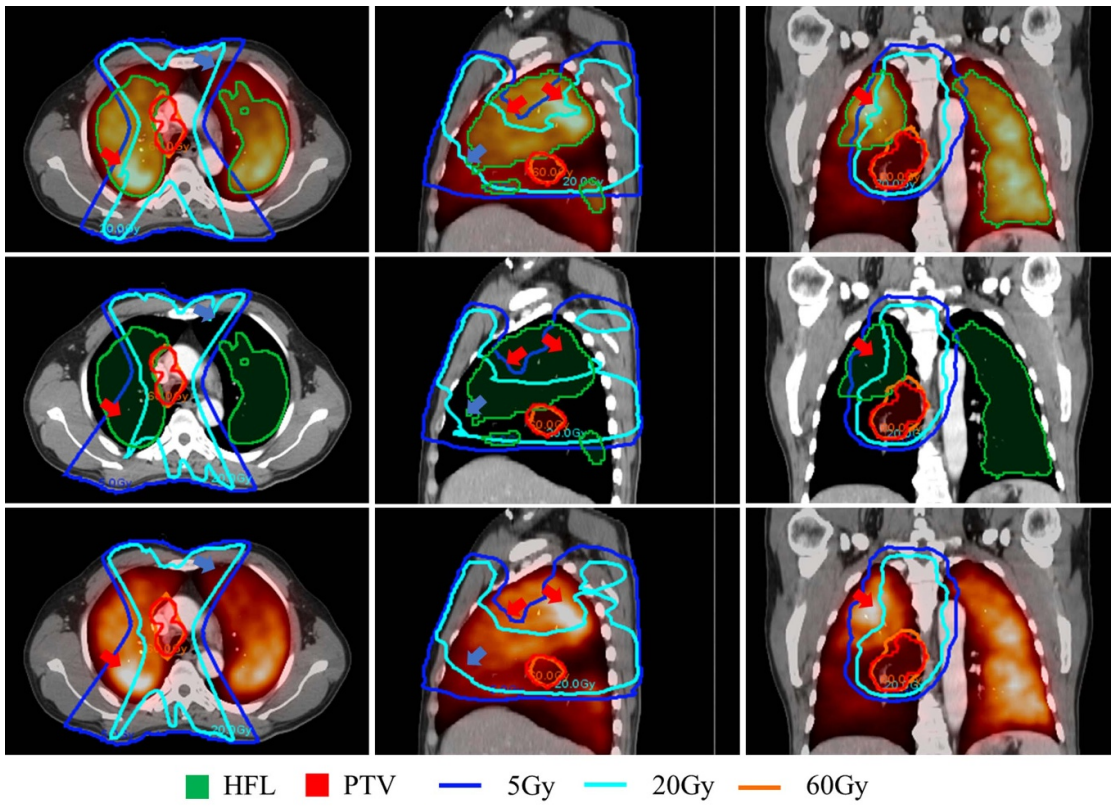

Figure 5. Comparison of iso-dose curves of 5 Gy (dark blue), 20 Gy (light blue), and 60 Gy (orange) between ConvRT (upper), cFLART (middle), and vFLART (lower) plans for an example case displayed in axial (left), sagittal (middle), and coronal (right) planes.

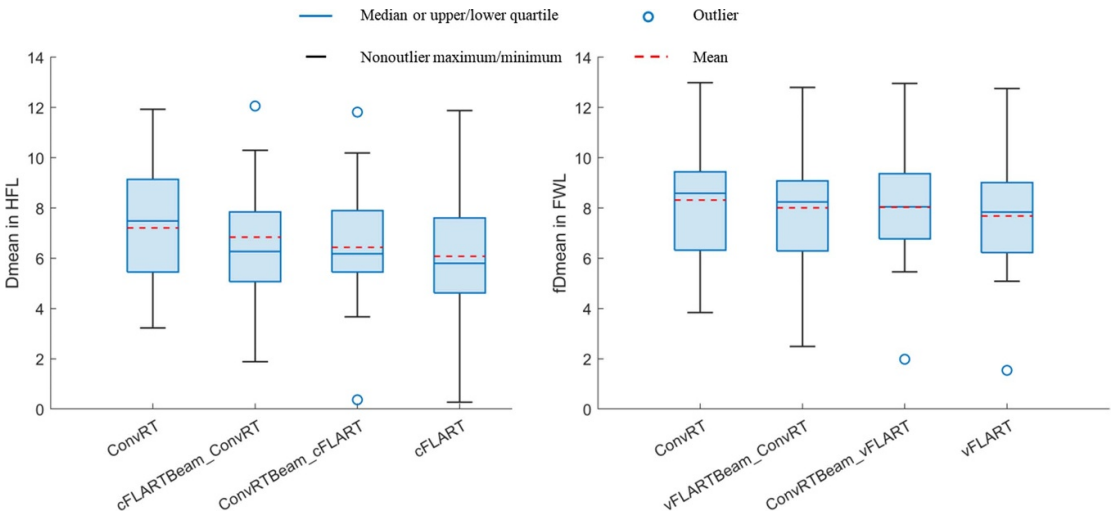

Figure 6. Results of the ablation studies including boxplots of HFL mean dose (left) and FWL functionally weighted mean dose (right).

large area of LFL benefit most from FLART plans while another study by Lavrenkov *et al* (2009) indicated that FLART plans are more beneficial in patients with non-uniform scattered-distributed LFL. These discrepancies may stem from the limited number of patient cases included in these studies and the plan variability caused by different planning strategies and different planners. AP-FLART alleviates these limitations by considerably lowering the barriers to including a larger dataset and ensuring plan consistency, thereby expediting the development of patient selection criteria and the standardization of FLART planning protocols.

Upon the establishment of FLART protocols, AP-FLART will boost the widespread clinical application of FLART. Considering the scarce clinical experience and the difficulties introduced by the complex and patient-specific lung function distributions in FLART planning (Faught *et al* 2018), it is of clinical significance for AP-FLART to assist beam angle selection and plan optimization. In this study, we utilized a specific FLART planning strategy including SPECT perfusion-based lung function imaging, threshold segmentation-based HFL, and linear weighting-based FWL to demonstrate the feasibility and effectiveness of AP-FLART. Nevertheless, it is anticipated to be still effective when using other strategies whichever are adopted by the protocol without much modification. It can accommodate other lung function imaging modalities such as CT-based perfusion/ventilation images (Ren *et al* 2021, Chen *et al* 2023, Li *et al* 2023), other HFL definitions such as homogeneity deviation-based HFL (Faught *et al* 2018), and other FWL definitions such as nonlinear weighting-based FWL (Faught *et al* 2017). Furthermore, when the benefits of minimizing functional dose metrics become more evident, the weights of functional dose metrics in the beam and plan scores can be increased to divert more doses away from HFL.

A few limitations exist in this study. First, the validation of AP-FLART's effectiveness was conducted on a limited dataset of 18 cases from a single center because data containing both RT and lung function imaging is scarce. Future studies will assess its performance on a larger multi-center dataset. Besides, the dose redirection principle presupposes that low function regions can be compromised. However, recent studies revealed that temporary lung function defects exist and their function may recover after or during treatment (Yuan *et al* 2012), necessitating future investigations to identify such temporary defects pretreatment and protect them when making treatment plans. Additionally, the use of free-breathing images fails to fully capture the influence of respiratory motion on the derived lung function maps (Huang *et al* 2022b), and the imperfect registration between SPECT and planning CT images may result in inconsistencies between the generated and actual lung function maps (Yin *et al* 2010). However, the proposed AP-FLART is also applicable to other lung function mapping techniques that may mitigate these challenges. Currently, AP-FLART is implemented in the open-source TPS matRad to demonstrate its technical feasibility and efficacy. Although we have adopted the dose mimicking algorithm to convert manual Eclipse plans into matRad plans for consistent comparison, there might still be some unaccounted differences since the reference manual plans were originally made using Eclipse TPSs. Future work will integrate the AP-FLART algorithm into clinical TPSs, such as Eclipse and RayStation to enable direct clinical evaluation. Implementing AP-FLART in clinical TPSs can also reduce planning time and facilitate broader clinical application through their efficient and well-validated dose calculation and plan optimization engines.

5. Conclusion

In this study, a novel AP-FLART was developed and validated. It integrates and enhances a dosimetric score-based beam angle selection method and a meta-optimization-based plan hyperparameter optimization approach. AP-FLART demonstrates the ability to generate RT plans of similar quality to manual plans within clinically acceptable time. Furthermore, AP-FLART can incorporate lung function information, employing either contour-based or voxel-based strategies, to redirect doses from high function regions to low function regions without severely damaging conventional dose metrics. The effective dose redirection is jointly driven by function-guided beam angle selection and plan optimization. AP-FLART is of potential to improve FLART planning efficiency, consistency, and quality, and advance the research and clinical application of FLART.

Data availability statement

The data cannot be made publicly available upon publication because they contain sensitive personal information. The data that support the findings of this study are available upon reasonable request from the authors.

Acknowledgments

This work was supported in part by General Research Fund (GRF 15103520) from the University Grants Committee, and Health and Medical Research Fund (HMRF 07183266) from the Food and Health Bureau, The Government of the Hong Kong Special Administrative Regions. This work was also supported in part by Henan provincial Medical Science and Technology Research Project (SBGJ202102056 and SBGJ202103038), Natural Science Foundation of Henan Province of China (222300420575 and 232300420231), Key Technologies R&D Programme of Henan Province (222102310015) and Overseas Study Personnel Research Excellence Funding and Entrepreneurship Start-up Project of Henan Province (37). The authors gratefully

acknowledge the insightful discussions about the MetaPlanner provided by Dr. Charles Huang from Department of Bioengineering of Stanford University.

Appendix A. Parameter determination for beam angle selection

The dosimetric score-based beam angle selection method involves several parameters to be determined. They include the weights of different regions to be protected in the beam score function and the weight and regularization parameter of the beam span term. For ConvRT, the weights for spinal cord, esophagus, heart, and normal tissues were set following Yuan *et al.* The weights for lung and the beam span term were fine-tuned by using a grid search method to minimize a plan score function. This function differs from that in the plan hyperparameter optimization by substituting the clipped linear relationship between the score values and the quality metric values with an exponential linear function defined by the equation (A1) to better align with clinical plan evaluation preferences,

$$F_{QM} = \begin{cases} \exp\left(\frac{QM-QM_+}{QM_+-QM_-}\right), & QM \geqslant QM_+ \\ \frac{QM-QM_-}{QM_+-QM_-}, & QM_- < QM < QM_+ \\ \exp\left(\frac{QM-QM_-}{QM_+-QM_-}\right) - 1, & QM \leqslant QM_- \end{cases}. \tag{A1}$$

As for FLART, all parameters excluding the lung weight were aligned with those used in ConvRT to maintain the relative importance of other OARs. The functional lung weight was fine-tuned to minimize functional dose metrics while preserving conventional dose metrics compared to ConvRT, which can be formulated as:

$$\min_{w} \quad d(w) = \frac{1}{N \bullet M} \sum_{i} \sum_{QM} \frac{QM_i^{FLART} - QM_i^{ConvRT}}{QM_i^{ConvRT}} \tag{A2}$$

where d stands for the relative differences between FLART and ConvRT plan quality metrics. QM represents quality metrics involved in the definition of the plan score function. QM_i^{FLART} and QM_i^{ConvRT} refer to the quality metric value of ith case in FLART and ConvRT plans respectively. N and M are the number of cases and quality metrics. w refers to the functional lung weight. The voxel size of dose grid was set to be $3 \times 3 \times 3$ mm^3 for final plan generation to accelerate the parameter search process.

Figure A1 presents the outcomes of the grid search optimization for beam angle selection parameters, with the optimal values detailed in table A1. The chosen weight for the beam span term is lower than the value suggested by Yuan *et al.* It can be attributed to the use of solely coplanar beams in this study, in contrast to the inclusion of non-coplanar beams in Yuan *et al* allowing for more varied beam distribution. The weight of FWL in vFLART is slightly higher than that of anatomical lungs in ConvRT. The contralateral lung usually has higher function and lower doses in lung RT plans due to the relatively far distance from the tumor. Consequently, FWL doses are usually lower than mean lung doses. A higher FWL weight can compensate for the lower dose values to maintain the relative importance of the anatomical/functional lung term in the beam score.

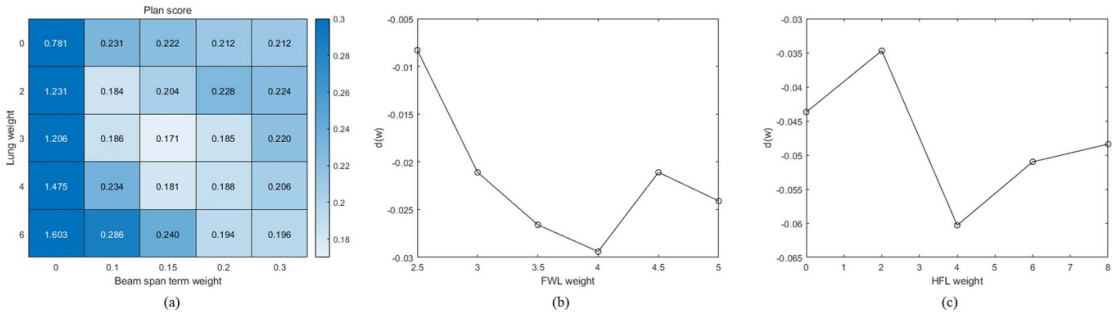

Figure A1. The grid search results for determining beam angle selection parameters.

Table A1. The determined parameters for beam angle selection.

Term	Spinal cord	Esophagus	Heart	Normal tissue	Lung	FWL	HFL	Beam span
ConvRT	10	0.3	0.3	0.15	3	0	0	0.15
vFLART	10	0.3	0.3	0.15	0	4	0	0.15
cFLART	10	0.3	0.3	0.15	2	0	4	0.15

Appendix B. Nearest initialization for plan hyperparameter optimization

The meta-optimization framework for plan hyperparameter optimization consists of two nested loops of optimization (Huang *et al* 2022a). For each iteration of the outer loop, dose objective weight configurations are updated and then FMO is performed to generate corresponding Pareto optimal plans. In essence, FMO solves a convex optimization problem using an iterative optimization algorithm, Interior Point OPTimizer (IPOPT). In the original meta-optimization framework, FMO initializes fluence maps with all one initialization. In this study, we propose a nearest initialization approach to accelerate the meta-optimization framework as illustrated by figure A2. For a new dose objective weight configuration to be computed, the nearest computed weight configuration defined by Euclidean distance will be sought, and its FMO result will serve as the initialization point of the new configuration's FMO. Since the optimal fluence maps resulted from FMO depend continuously on the weight configurations (Monz *et al* 2008), the nearest initialization approach shall reduce the iteration time for IPOPT to reach global optimal point compared to the original all one initialization method and thus accelerate the optimization process.

A comparison study was conducted to demonstrate the effectiveness of the nearest initialization approach. We generated two ConvRT plans for each collected case using the proposed AP-FLART with all one initialization and the nearest initialization respectively. The results showed that the mean iteration number per FMO was 121 versus 33. The computation time spent on FMO was 61.21 $\pm$ 18.15 min per plan when using all one initialization versus 22.55 $\pm$ 6.91 min per plan when using the nearest initialization, indicating a time reduction of 63%.

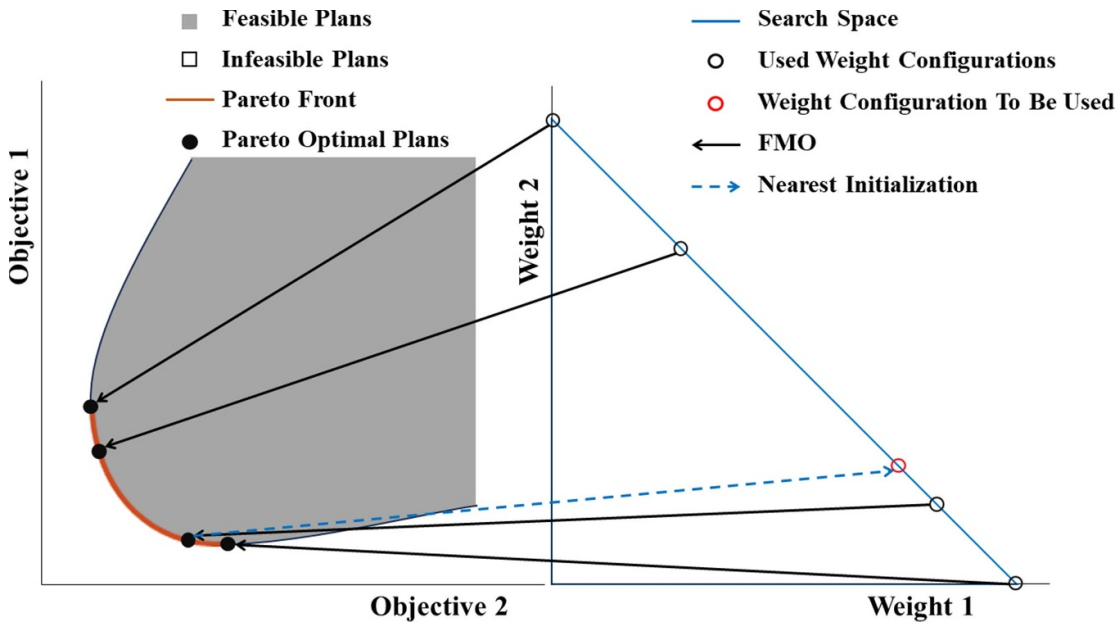

Figure A2. Illustration of the nearest initialization for the meta-optimization-based plan hyperparameter optimization.

Appendix C. Dose mimicking for plan conversion

The dose mimicking algorithm aims to produce deliverable treatment plans that mimic or even improve given dose distribution. In this study, we utilize the voxel-based dose mimicking algorithm (McIntosh *et al* 2017, Fan *et al* 2019) to generate matRad plans that can have similar or even better dose distribution compared to their Eclipse counterparts. The dose mimicking algorithm can be formulated as follows (McIntosh *et al* 2017):

$$\begin{aligned} &\min_{x} \quad \sum_{i\in \mathrm{PTV}} \left(d_i^{\mathrm{cal}} - d_i^{\mathrm{ref}}\right)^2 + \sum_{i\in \mathit{Body\,minus\,PTV}} H\left(d_i^{\mathrm{cal}} - d_i^{\mathrm{ref}}\right)\left(d_i^{\mathrm{cal}} - d_i^{\mathrm{ref}}\right)^2 \\ &\text{s.t.} \quad x \geqslant 0 \\ &\quad \overrightarrow{d^{\mathrm{cal}}} = D\vec{x} \end{aligned} \tag{A3}$$

where $\vec{x}$, D, and $\overrightarrow{d^{\mathrm{cal}}}$ refer to the fluence map, the dose influence matrix, and the calculated dose distribution respectively. $\overrightarrow{d^{\mathrm{ref}}}$ stands for the reference dose distribution, i.e. the planning dose distribution of manual Eclipse plans. H represents the Heaviside function. The IPOPT of matRad is applied to solve the above optimization problem to obtain optimal fluence map. Leaf sequencing and direct aperture optimization are then performed to generate final plans. The dose calculation and plan optimization algorithms used in the dose mimicking process are the same as those used in AP-FLART. The dose mimicking results are shown in table A2.

Compared to original Eclipse plans, mimicked matRad plans have significantly lower doses to all OARs including lung, spinal cord, esophagus, and heart. The lower OAR doses can be attributed to the compromise in PTV homogeneity and conformity, and the different dose calculation and plan optimization algorithms. For example, the PB dose calculation algorithm tends to underestimate doses to OAR regions which are distant from beam paths for lung RT plans (Elcim *et al* 2018). This is because the PB algorithm lacks the inhomogeneity correction for the lateral scattering and lung has a low density (Elcim *et al* 2018).

Table A2. Comparison between original Eclipse plans and converted matRad plans through dose mimicking. The mean and standard deviation of the dose metrics over all collected cases are listed. The p-values by Wilcoxon signed-rank test are also shown.

	HI	CI	PTV D_1 (Gy)	HFL D_{mean} (Gy)	HFL V_{20} (%)	HFL V_5 (%)	FWL fD_{mean} (Gy)	FWL fV_{20} (%)	FWL fV_5 (%)	Lung D_{mean} (Gy)
Original plans	5.95 ± 1.42	0.65 ± 0.07	63.99 ± 0.98	8.09 ± 2.58	12.87 ± 6.37	29.81 ± 9.73	9.44 ± 2.45	15.54 ± 5.70	33.76 ± 8.64	11.31 ± 2.16
Converted plans	6.71 ± 1.76	0.63 ± 0.09	64.61 ± 1.17	7.17 ± 2.48	12.88 ± 5.66	26.63 ± 9.03	8.62 ± 2.51	15.75 ± 5.61	30.66 ± 8.08	10.59 ± 2.12
p-value	0.005	0.468	0.007	<0.001	1.000	0.003	<0.001	0.671	0.005	<0.001
	Lung V_{20} (%)	Lung V_5 (%)	SpinalCord D_{max} (Gy)	Esophagus D_{mean} (Gy)	Esophagus D_1 (Gy)	Heart D_{mean} (Gy)	Heart D_1 (Gy)	Heart V_{40} (%)	Body D_{mean} (Gy)	
Original plans	19.45 ± 4.46	38.00 ± 7.00	39.30 ± 6.12	16.94 ± 8.37	54.09 ± 15.61	9.82 ± 7.47	45.39 ± 17.72	6.31 ± 6.85	5.66 ± 1.78	
Converted plans	19.73 ± 4.44	35.05 ± 5.76	36.63 ± 3.95	13.32 ± 6.39	50.93 ± 17.26	7.37 ± 5.95	39.27 ± 17.33	1.92 ± 2.19	4.91 ± 1.48	
p-value	0.671	0.010	0.003	<0.001	0.038	<0.001	<0.001	<0.001	<0.001	

Appendix D. Detailed results of ablation studies

Table A3. The detailed results of the ablation studies. The mean and standard deviation of the dose metrics over all collected cases are listed. The *p*-values by Wilcoxon signed-rank test are also shown.

				p-value			*p*-value	
Dose metrics	ConvRT	cFLART	cFLARTBeam_ConvRT	VS ConvRT	VS cFLART	ConvRTBeam_cFLART	VS ConvRT	VS cFLART
HI	5.56 ± 0.51	5.61 ± 0.52	5.61 ± 0.60	0.671	1.000	5.62 ± 0.49	0.495	0.932
CI	0.76 ± 0.06	0.72 ± 0.06	0.74 ± 0.08	0.081	0.099	0.74 ± 0.07	0.369	0.054
PTV D_1 (Gy)	63.93 ± 0.35	64.01 ± 0.41	63.96 ± 0.46	0.932	0.609	64.01 ± 0.34	0.304	1.000
HFL D_{mean} (Gy)	7.21 ± 2.28	6.08 ± 2.44	6.84 ± 2.32	0.099	<0.001	6.43 ± 2.50	<0.001	0.007
HFL V_{20} (%)	13.01 ± 5.55	11.00 ± 5.75	12.80 ± 5.92	0.304	<0.001	11.26 ± 5.92	0.001	0.369
HFL V_5 (%)	32.64 ± 10.50	25.98 ± 9.32	28.11 ± 7.70	0.018	0.002	29.66 ± 11.59	0.010	0.008
FWL fD_{mean} (Gy)	8.32 ± 2.22	7.76 ± 2.44	8.15 ± 2.30	0.468	0.001	7.92 ± 2.44	0.054	0.142
FWL fV_{20} (%)	15.18 ± 5.23	14.71 ± 5.57	15.48 ± 5.67	0.766	0.054	14.48 ± 5.43	0.167	0.130
FWL fV_5 (%)	35.92 ± 9.27	30.69 ± 9.16	32.47 ± 7.56	0.024	0.003	33.51 ± 10.81	0.060	0.024
Lung D_{mean} (Gy)	10.04 ± 2.11	10.05 ± 1.88	10.10 ± 2.02	0.468	0.932	10.01 ± 1.89	1.000	0.671
Lung V_{20} (%)	18.74 ± 4.59	19.56 ± 4.09	19.43 ± 4.65	0.284	0.495	18.88 ± 4.01	0.702	0.002
Lung V_5 (%)	39.79 ± 8.61	36.55 ± 7.74	37.83 ± 7.66	0.074	0.014	38.30 ± 8.31	0.181	0.060
SpinalCord D_{max} (Gy)	37.69 ± 6.8 6	38.01 ± 5.59	36.73 ± 5.87	0.099	0.007	38.64 ± 5.60	0.060	0.229
Esophagus D_{mean} (Gy)	13.29 ± 8.38	12.05 ± 7.80	12.80 ± 8.18	0.099	0.142	12.27 ± 7.90	0.054	0.417
Esophagus D_1 (Gy)	49.80 ± 21.81	48.86 ± 21.94	49.46 ± 21.66	0.229	0.702	49.36 ± 21.72	0.369	0.154
Heart D_{mean} (Gy)	6.37 ± 6.21	6.69 ± 6.38	6.34 ± 6.24	0.181	0.495	6.17 ± 5.85	0.229	0.016
Heart D_1 (Gy)	33.41 ± 23.82	33.88 ± 23.96	33.77 ± 23.23	0.081	0.442	32.93 ± 23.73	0.284	0.014
Heart V_{40} (%)	2.29 ± 2.86	2.47 ± 3.39	2.30 ± 2.89	0.969	0.784	2.12 ± 2.94	0.092	0.014
Body D_{mean} (Gy)	4.78 ± 1.55	4.76 ± 1.49	4.75 ± 1.50	0.142	0.766	4.78 ± 1.54	0.865	0.369

(Continued.)

Table A3. (Continued.)

Dose metrics	ConvRT	vFLART	vFLARTBeam_ConvRT	*p*-value		ConvRTBeam_vFLART	*p*-value	
				VS ConvRT	VS vFLART		VS ConvRT	VS vFLART
HI	5.56 ± 0.51	5.55 ± 0.54	5.59 ± 0.61	1.000	0.702	5.59 ± 0.54	0.799	0.832
CI	0.76 ± 0.06	0.71 ± 0.08	0.73 ± 0.08	0.027	0.081	0.75 ± 0.07	0.229	0.005
PTV D_1 (Gy)	63.93 ± 0.35	63.96 ± 0.43	63.94 ± 0.43	0.865	0.766	63.96 ± 0.43	0.734	0.832
HFL D_{mean} (Gy)	7.21 ± 2.28	6.18 ± 2.39	6.66 ± 2.38	0.009	<0.001	6.76 ± 2.37	0.024	<0.001
HFL V_{20} (%)	13.01 ± 5.55	11.14 ± 5.60	12.43 ± 5.73	0.081	0.001	11.55 ± 5.95	0.027	0.167
HFL V_5 (%)	32.64 ± 10.50	26.30 ± 12.22	26.81 ± 8.96	0.006	0.024	31.74 ± 13.88	0.108	<0.001
FWL fD_{mean} (Gy)	8.32 ± 2.22	7.68 ± 2.37	8.01 ± 2.30	0.099	0.008	8.03 ± 2.35	0.108	<0.001
FWL fV_{20} (%)	15.18 ± 5.23	14.28 ± 5.55	15.15 ± 5.40	0.702	0.030	14.22 ± 5.66	0.119	0.671
FWL fV_5 (%)	35.92 ± 9.27	30.85 ± 10.87	31.42 ± 8.03	0.009	0.012	35.22 ± 12.27	0.167	<0.001
Lung D_{mean} (Gy)	10.04 ± 2.11	9.94 ± 2.04	9.98 ± 2.02	0.932	0.393	10.02 ± 2.03	0.551	0.196
Lung V_{20} (%)	18.74 ± 4.59	19.18 ± 4.77	19.19 ± 4.31	0.551	0.702	18.56 ± 4.80	0.766	0.038
Lung V_5 (%)	39.79 ± 8.61	36.26 ± 7.75	36.77 ± 7.25	0.081	0.021	39.36 ± 8.58	0.167	0.006
SpinalCord D_{max} (Gy)	37.69 ± 6.86	37.63 ± 6.47	36.90 ± 6.48	0.054	0.067	37.87 ± 6.60	0.417	0.766
Esophagus D_{mean} (Gy)	13.29 ± 8.38	12.91 ± 8.07	12.89 ± 8.18	0.246	0.671	13.19 ± 8.13	0.284	0.167
Esophagus D_1 (Gy)	49.80 ± 21.81	49.84 ± 20.23	49.69 ± 21.44	0.284	0.551	49.82 ± 20.54	0.154	0.640
Heart D_{mean} (Gy)	6.37 ± 6.21	7.03 ± 6.33	6.49 ± 6.43	0.142	0.734	6.52 ± 5.86	0.196	0.027
Heart D_1 (Gy)	33.41 ± 23.82	34.67 ± 23.71	34.22 ± 23.61	0.067	0.523	33.77 ± 23.12v	0.468	0.081
Heart V_{40} (%)	2.29 ± 2.86	2.49 ± 3.02	2.42 ± 3.01	0.556	0.724	1.85 ± 2.30	0.108	0.005
Body D_{mean} (Gy)	4.78 ± 1.55	4.73 ± 1.50	4.72 ± 1.49	0.034	0.671	4.78 ± 1.55	0.899	0.043

ORCID iDs

Tianyu Xiong https://orcid.org/0000-0001-5546-8039
Yu-Hua Huang https://orcid.org/0000-0001-9610-2113
Xi Liu https://orcid.org/0009-0009-6924-4525
Ge Ren https://orcid.org/0000-0003-2049-2682

References

Amit G, Purdie T G, Levinshtein A, Hope A J, Lindsay P, Marshall A, Jaffray D A and Pekar V 2015 Automatic learning-based beam angle selection for thoracic IMRT *Med. Phys.* **42** 1992–2005
Bedford J L and Ahmed M 2023 Functional lung avoidance in radiotherapy using optimisation of biologically effective dose with non-coplanar beam orientations *Phys. Imaging Radiat. Oncol.* **28** 100518
Bortfeld T, Schlegel W and Rhein B 1993 Decomposition of pencil beam kernels for fast dose calculations in three-dimensional treatment planning *Med. Phys.* **20** 311–8
Bradley J D *et al* 2015 Standard-dose versus high-dose conformal radiotherapy with concurrent and consolidation carboplatin plus paclitaxel with or without cetuximab for patients with stage IIIA or IIIB non-small-cell lung cancer (RTOG 0617): a randomised, two-by-two factorial phase 3 study *Lancet Oncol.* **16** 187–99
Bria W F, Kanarek D J and Kazemi H 1983 Prediction of postoperative pulmonary function following thoracic operations. Value of ventilation-perfusion scanning *J. Thorac. Cardiovasc. Surg.* **86** 186–92
Bucknell N W, Hardcastle N, Bressel M, Hofman M S, Kron T, Ball D and Siva S 2018 Functional lung imaging in radiation therapy for lung cancer: a systematic review and meta-analysis *Radiother. Oncol.* **129** 196–208
Chen Z, Huang Y-H, Kong F-M, Ho W Y, Ren G and Cai J 2023 A super-voxel-based method for generating surrogate lung ventilation images from CT *Front. Physiol.* **14** 1085158
Christian J A, Partridge M, Nioutsikou E, Cook G, McNair H A, Cronin B, Courbon F, Bedford J L and Brada M 2005 The incorporation of SPECT functional lung imaging into inverse radiotherapy planning for non-small cell lung cancer *Radiother. Oncol.* **77** 271–7
Elcim Y, Dirican B and Yavas O 2018 Dosimetric comparison of pencil beam and Monte Carlo algorithms in conformal lung radiotherapy *J. Appl. Clin. Med. Phys.* **19** 616–24
Fan J, Wang J, Chen Z, Hu C, Zhang Z and Hu W 2019 Automatic treatment planning based on three-dimensional dose distribution predicted from deep learning technique *Med. Phys.* **46** 370–81
Faught A M, Olsen L, Schubert L, Rusthoven C, Castillo E, Castillo R, Zhang J, Guerrero T, Miften M and Vinogradskiy Y 2018 Functional-guided radiotherapy using knowledge-based planning *Radiother. Oncol.* **129** 494–8
Faught A M, Yamamoto T, Castillo R, Castillo E, Zhang J, Miften M and Vinogradskiy Y 2017 Evaluating which dose-function metrics are most critical for functional-guided radiation therapy *Int. J. Radiat. Oncol. Biol. Phys.* **99** 202–9
Ge Y and Wu Q J 2019 Knowledge-based planning for intensity-modulated radiation therapy: a review of data-driven approaches *Med. Phys.* **46** 2760–75
Hanania A N, Mainwaring W, Ghebre Y T, Hanania N A and Ludwig M 2019 Radiation-induced lung injury: assessment and management *Chest* **156** 150–62
Hoover D A, Reid R H, Wong E, Stitt L, Sabondjian E, Rodrigues G B, Jaswal J K and Yaremko B P 2014 SPECT-based functional lung imaging for the prediction of radiation pneumonitis: a clinical and dosimetric correlation *J. Med. Imaging Radiat. Oncol.* **58** 214–22
Huang C, Nomura Y, Yang Y and Xing L 2022a Meta-optimization for fully automated radiation therapy treatment planning *Phys. Med. Biol.* **67** 055011
Huang T C, Hsiao C Y, Chien C R, Liang J A, Shih T C and Zhang G G 2013 IMRT treatment plans and functional planning with functional lung imaging from 4D-CT for thoracic cancer patients *Radiat. Oncol.* **8** 3
Huang Y-H, Ren G, Xiao H, Yang D, Kong F-M, Ho W Y and Cai J 2022b Volumetric multiphase ventilation imaging based on four-dimensional computed tomography for functional lung avoidance radiotherapy *Med. Phys.* **49** 7237–46
Ireland R H, Tahir B A, Wild J M, Lee C E and Hatton M Q 2016 Functional image-guided radiotherapy planning for normal lung avoidance *Clin. Oncol.* **28** 695–707
Khalil A A *et al* 2021 Personal innovative approach in radiation therapy of lung cancer- functional lung avoidance SPECT-guided (ASPECT) radiation therapy: a study protocol for phase II randomised double-blind clinical trial *BMC Cancer* **21** 940
Lavrenkov K, Singh S, Christian J A, Partridge M, Nioutsikou E, Cook G, Bedford J L and Brada M 2009 Effective avoidance of a functional spect-perfused lung using intensity modulated radiotherapy (IMRT) for non-small cell lung cancer (NSCLC): an update of a planning study *Radiother. Oncol.* **91** 349–52
Lee D and Wiswall M 2007 A parallel implementation of the simplex function minimization routine *Comput. Econ.* **30** 171–87
Li S, Liu J, Gao S, Yin Y, Zhang L, Han Y, Zhang X, Li Y, Yan J and Hou Z 2023 CT ventilation image-guided helical tomotherapy at sparing functional lungs for locally advanced lung cancer: analysis of dose-function metrics and the impact on pulmonary toxicity *Radiat. Oncol.* **18** 6
Matuszak M M, Matrosic C, Jarema D, McShan D L, Stenmark M H, Owen D, Jolly S, Kong F-M (Spring) and Ten Haken R K 2016 Priority-driven plan optimization in locally advanced lung patients based on perfusion SPECT imaging *Adv. Radiat. Oncol.* **1** 281–9
McGuire S M, Marks L B, Yin F F and Das S K 2010 A methodology for selecting the beam arrangement to reduce the intensity-modulated radiation therapy (IMRT) dose to the SPECT-defined functioning lung *Phys. Med. Biol.* **55** 403
McGuire S M, Zhou S, Marks L B, Dewhirst M, Yin F F and Das S K 2006 A methodology for using SPECT to reduce intensity-modulated radiation therapy (IMRT) dose to functioning lung *Int. J. Radiat. Oncol. Biol. Phys.* **66** 1543–52
McIntosh C, Welch M, McNiven A, Jaffray D A and Purdie T G 2017 Fully automated treatment planning for head and neck radiotherapy using a voxel-based dose prediction and dose mimicking method *Phys. Med. Biol.* **62** 5926
Meyer J, Hummel S M, Cho P S, Austin-Seymour M M and Phillips M H 2005 Automatic selection of non-coplanar beam directions for three-dimensional conformal radiotherapy *Br. J. Radiol.* **78** 316–27
Monz M, Küfer K H, Bortfeld T R and Thieke C 2008 Pareto navigation: algorithmic foundation of interactive multi-criteria IMRT planning *Phys. Med. Biol.* **53** 985–98
Moore K L 2019 Automated radiotherapy treatment planning *Sem. Radiat. Oncol.* **29** 209–18

Munawar I et al 2010 Intensity modulated radiotherapy of non-small-cell lung cancer incorporating SPECT ventilation imaging *Med. Phys.* **37** 1863–72
Nelder J A and Mead R 1965 A simplex method for function minimization *Comput. J.* **7** 308–13
Ren G, Zhang J, Li T, Xiao H, Cheung L Y, Ho W Y, Qin J and Cai J 2021 Deep learning-based computed tomography perfusion mapping (DL-CTPM) for pulmonary CT-to-perfusion translation *Int. J. Radiat. Oncol. Biol. Phys.* **110** 1508–18
Siochi R A C 1999 Minimizing static intensity modulation delivery time using an intensity solid paradigm *Int. J. Radiat. Oncol. Biol. Phys.* **43** 671–80
Sung H, Ferlay J, Siegel R L, Laversanne M, Soerjomataram I, Jemal A and Bray F 2021 Global cancer statistics 2020: GLOBOCAN estimates of incidence and mortality worldwide for 36 cancers in 185 countries *CA Cancer J. Clin.* **71** 209–49
Tahir B A, Bragg C M, Wild J M, Swinscoe J A, Lawless S E, Hart K A, Hatton M Q and Ireland R H 2017 Impact of field number and beam angle on functional image-guided lung cancer radiotherapy planning *Phys. Med. Biol.* **62** 7114
Thai A A, Solomon B J, Sequist L V, Gainor J F and Heist R S 2021 Lung cancer *Lancet* **398** 535–54
Vinod S K and Hau E 2020 Radiotherapy treatment for lung cancer: current status and future directions *Respirology* **25** 61–71
Vinogradskiy Y et al 2022 Results of a multi-institutional phase 2 clinical trial for 4DCT-ventilation functional avoidance thoracic radiation therapy *Int. J. Radiat. Oncol. Biol. Phys.* **112** 986–95
Wieser H-P et al 2017 Development of the open-source dose calculation and optimization toolkit matRad *Med. Phys.* **44** 2556–68
Yamamoto T et al 2023 Four-dimensional computed tomography ventilation image-guided lung functional avoidance radiation therapy: a single-arm prospective pilot clinical trial *Int. J. Radiat. Oncol. Biol. Phys.* **115** 1144–54
Yamamoto T, Kabus S, Bal M, Keall P, Benedict S and Daly M 2016 The first patient treatment of computed tomography ventilation functional image-guided radiotherapy for lung cancer *Radiother. Oncol.* **118** 227–31
Yamamoto T, Kabus S, von Berg J, Lorenz C and Keall P J 2011 Impact of four-dimensional computed tomography pulmonary ventilation imaging-based functional avoidance for lung cancer radiotherapy *Int. J. Radiat. Oncol. Biol. Phys.* **79** 279–88
Yaremko B P et al 2022 Functional lung avoidance for individualized radiation therapy: results of a double-masked, randomized controlled trial *Int. J. Radiat. Oncol. Biol. Phys.* **113** 1072–84
Yin L S et al 2010 Complexity and accuracy of image registration methods in SPECT-guided radiation therapy *Phys. Med. Biol.* **55** 237
Yuan L, Wu Q J, Yin F, Li Y, Sheng Y, Kelsey C R and Ge Y 2015 Standardized beam bouquets for lung IMRT planning *Phys. Med. Biol.* **60** 1831–43
Yuan L, Zhu W, Ge Y, Jiang Y, Sheng Y, Yin -F-F and Wu Q J 2018 Lung IMRT planning with automatic determination of beam angle configurations *Phys. Med. Biol.* **63** 135024
Yuan S T et al 2012 Changes in global function and regional ventilation and perfusion on SPECT during the course of radiotherapy in patients with non-small-cell lung cancer *Int. J. Radiat. Oncol. Biol. Phys.* **82** e631–8
Zhou P X and Zhang S X 2022 Functional lung imaging in thoracic tumor radiotherapy: application and progress *Front. Oncol.* **12** 908345